MOLECULAR IMAGING AND BIOLOGY

Mol Imaging Biol (2017) 19:531–539
DOI: 10.1007/s11307-016-1036-8

Published Online: 15 December 2016

RESEARCH ARTICLE

Immunoglobulin G (IgG)-Based Imaging Probe Accumulates in M1 Macrophage-Infiltrated Atherosclerotic Plaques Independent of IgG Target Molecule Expression

Yoichi Shimizu,[1,2] Hiroko Hanzawa,[3] Yan Zhao,[4] Sagiri Fukura,[4] Ken-ichi Nishijima,[2,4] Takeshi Sakamoto,[5] Songji Zhao,[4] Nagara Tamaki,[4] Mikako Ogawa,[1] Yuji Kuge[2,4]

[1]*Laboratory of Bioanalysis and Molecular Imaging, Faculty of Pharmaceutical Sciences, Hokkaido University, Kita 12 Nishi 6, Kita-ku, Sapporo, 060-0812, Japan*
[2]*Central Institute of Isotope Science, Hokkaido University, Kita 15 Nishi 7, Kita-ku, Sapporo, 060-0815, Japan*
[3]*Center for Exploratory Research, Research & Development Group, Hitachi, Ltd, Hatoyama, 350-0395, Japan*
[4]*Hokkaido University Graduate School of Medicine, Kita 15 Nishi 7, Kita-ku, Sapporo, 060-8638, Japan*
[5]*Center for Technology Innovation—Healthcare, Research & Development Group, Hitachi, Ltd., Kokubunji, 185-8601, Japan*

Abstract

Purpose: Vulnerable plaques are key factors for ischemic diseases. Thus, their precise detection is necessary for the diagnosis of such diseases. Immunoglobulin G (IgG)-based imaging probes have been developed for imaging biomolecules related to plaque formation for the diagnosis of atherosclerosis. However, IgG accumulates nonspecifically in atherosclerotic regions, and its accumulation mechanisms have not yet been clarified in detail. Therefore, we explored IgG accumulation mechanisms in atherosclerotic lesions and examined images of radiolabeled IgG for the diagnosis of atherosclerosis.

Procedures: Mouse IgG without specificity to biomolecules was labeled with technetium-99m via 6-hydrazinonicotinate to yield [^{99m}Tc]IgG. ApoE$^{-/-}$ or C57BL/6J mice were injected intravenously with [^{99m}Tc]IgG, and their aortas were excised 24 h after injection. After radioactivity measurement, serial aortic sections were autoradiographically and histopathologically examined. RAW264.7 macrophages were polarized into M1 or M2 and then treated with [^{99m}Tc]IgG. The radioactivities in the cells were measured after 1 h of incubation. [^{99m}Tc]IgG uptake in M1 macrophages was also evaluated after the pretreatment with an anti-Fcγ receptor (FcγR) antibody. The expression levels of FcγRs in the cells were measured by western blot analysis.

Results: [^{99m}Tc]IgG accumulation levels in the aortas were significantly higher in apoE$^{-/-}$ mice than in C57BL/6J mice (5.1 ± 1.4 vs 2.8 ± 0.5 %ID/g, $p < 0.05$). Autoradiographic images showed that the accumulation areas highly correlated with the macrophage-infiltrated areas. M1 macrophages showed significantly higher levels of [^{99m}Tc]IgG than M2 or M0 (nonpolarized) macrophages [2.2 ± 0.3 (M1) vs 0.5 ± 0.1 (M2), 0.4 ± 0.1 (M0) %dose/mg protein, $p < 0.01$] and higher expression levels of FcγRI and FcγRII. [^{99m}Tc]IgG accumulation

Electronic supplementary material The online version of this article (doi:10.1007/s11307-016-1036-8) contains supplementary material, which is available to authorized users.

Correspondence to: Yoichi Shimizu; *e-mail:* yshimizu@pharm.hokudai.ac.jp

in M1 macrophages was suppressed by pretreatment with the anti-FcγR antibody [2.2 ± 0.3 (nonpretreatment) vs 1.2 ± 0.2 (pretreatment) %ID/mg protein, $p < 0.01$].
Conclusions: IgG accumulated in pro-inflammatory M1 macrophages via FcγRs in atherosclerotic lesions. Thus, the target biomolecule-independent imaging of active inflammation should be taken into account in the diagnosis of atherosclerosis using IgG-based probes.

Key words: Nuclear imaging, Atherosclerosis, Macrophage, Polarization, Immunoglobulin G

Introduction

Atherosclerosis, especially in cases of vulnerable plaques, is a risk factor since plaque rupture and the following thrombogenesis induce ischemic diseases such as cerebral and myocardial infarctions [1]. Therefore, it is necessary to precisely detect vulnerable lesions for the diagnosis of such diseases. Various types of biomolecule are expressed or activated as atherosclerosis progresses [2–4]. Thus, the detection of those biomolecules in the lesions would make it possible to determine the extent of progression of atherosclerosis in detail.

For *in vivo* diagnosis of atherosclerosis, numerous approaches have been developed and advanced to be clinically useful for various imaging modalities especially nuclear imaging techniques including positron emission tomography (PET) and single-photon emission computed tomography (SPECT) [5–7]. For *in vivo* imaging of atherosclerotic plaques and monitoring the efficacy of therapy, various kinds of PET and SPECT imaging probes have been developed, for visualizing the expression or activity of biomolecules associated with atherosclerosis [8, 9]. To achieve target biomolecule-specific *in vivo* imaging in the diagnosis of atherosclerosis, immunoglobulin G (IgG)-based PET/SPECT imaging probes have been developed [10–12]. IgG has high and specific affinity to its target biomolecules through the antigen–antibody reaction [13], and it is comparatively easy to obtain the target IgG by established methods such as the phage display technique [14]. However, IgG accumulates nonspecifically in inflammatory regions [15, 16]. In fact, we found that our IgG probe accumulates in atherosclerotic lesions of apoE$^{-/-}$ mice (an atherosclerosis model) independent of its target biomolecule in our attempt to develop a novel SPECT imaging probe targeting a biomolecule specifically expressed in vulnerable lesions [17]. IgG has been reported to nonspecifically accumulate in infectious and inflammatory sites [18], which was considered to be due to the Fc domain of IgG [19]. Taking into account that atherosclerosis is a chronic disease, the nonspecific accumulation of an IgG-based probe might be due to its uptake by immune cells infiltrating the atherosclerotic lesions. However, certain issues, such as the types of immune cell in which IgG-based probes accumulate, remain to be clarified in detail.

In this study, to explore the IgG accumulation mechanisms in atherosclerotic lesions, we first examined the distribution of technetium-99m-labeled monoclonal IgG (hereafter, [^{99m}Tc]IgG) in apoE$^{-/-}$ mice. We found that [^{99m}Tc]IgG accumulated in the macrophage-infiltrated areas of atherosclerotic plaques. Thus, we next evaluated the relationship between [^{99m}Tc]IgG accumulation in macrophages and macrophage polarization and the expression of Fcγ receptors (FcγRs) which recognize the Fc domain of IgG. Finally, we elucidated where the IgG-based imaging probe itself distributes in the atherosclerotic state independent of the target biomolecules of IgG.

Materials and Methods

Materials

All the chemicals used in this study were commercially available and of the highest purity. 6-Hydrazinonicotinic acid (HYNIC)-*N*-hydroxysuccinimide was prepared as previously reported [20]. [^{99m}Tc]pertechnetate was purchased from Nihon Medi-Physics Co., Ltd. (Tokyo, Japan).

Preparation of Radiolabeled IgG ([^{99m}Tc]IgG)

As a nontargeting mouse IgG, we chose mouse IgG2b, kappa monoclonal [MG2b-57]-isotype control (Abcam, Cambridge, UK), whose immunogen is trinitrophenol keyhole limpet hemocyanin (KLH). IgG was radiolabeled with technetium-99m after derivatization with HYNIC as previously reported [21]. In brief, to HYNIC-*N*-hydroxysuccinimide in *N*,*N*-dimethylformamide (1 mg/ml, 8.25 μl), IgG solution in 0.16 M borate buffer (pH 8.0) (2 mg/ml, 250 μl) was added, and the mixture was incubated at room temperature for 2 h. The mixture was then purified by size exclusion filtration with a diafiltration membrane [Amicon Ultra 4 (molecular weight cutoff, 30,000); Millipore Co., Billerica, MA]. [^{99m}Tc](tricine)$_2$ (740 MBq/ml, 300 μl) prepared as previously reported [22] was added to the purified solution of the HYNIC-IgG solution in 10 mM citrate buffer (pH 5.2) (1 mg/ml, 30 μl) and incubated at room temperature for 1 h. The mixture was then purified on a Sephadex G-25 column (PD-10, GE Healthcare, Buckinghamshire, UK) equilibrated with 0.1 M phosphate-buffered saline (PBS) (pH 7.4) to obtain [^{99m}Tc]IgG. The radiochemical purity of [^{99m}Tc]IgG was measured by size exclusion filtration using a PD-10 column and by size exclusion high-performance liquid chromatography (HPLC). HPLC analysis was performed with a Shimadzu HPLC

gradient system (LC-20AD system; Shimadzu Corporation, Kyoto, Japan) monitored using a UV detector at 280 nm and a radiodetector (RLC-700, Hitachi Aloka, Medical, Tokyo, Japan) equipped with a TSK gel SW3000 column (Tosoh Bioscience, Tokyo, Japan) and equilibrated with 0.1 M phosphate buffer (pH 6.8) at a flow rate of 0.2 ml/min. To evaluate the stability of [^{99m}Tc]IgG, the probe (34.9 MBq/ml, 50 µl) was incubated with the plasma (50 µl) derived from C57BL/6J mice (male, 30 weeks) for 24 h, and then, the mixture was analyzed by size exclusion filtration using the PD-10 column.

Animal Study

As previously described by Shimizu et al. [17], animal care and all experimental procedures were performed with the approval of the animal care committee of Hokkaido University. The studies were performed on male apoE$^{-/-}$ mice obtained from the Taconic Gnotobiotic Center (NY, USA) and C57BL/6J mice obtained from Charles River Japan Inc. (Kanagawa, Japan). The animals were kept in a temperature-controlled facility in the laboratory of animal experiments at the Institute for Animal Experimentation, Graduate School of Medicine, Hokkaido University on a 12-h light cycle with free access to food and water. At 5 weeks of age, the mice were maintained on a high-fat diet (21 % fat, 0.15 % cholesterol, no cholate; obtained from Oriental Yeast Co., Ltd.). At 35 weeks of age, the animals (n = 4/group) were anesthetized with pentobarbital (0.025 mg/kg body weight, intraperitoneally). [^{99m}Tc]IgG (481–962 kBq/2 µg/100 µl of PBS(−) per mouse) was intravenously injected to the mice. Twenty-four hours after the injection, the animals were euthanized under pentobarbital anesthesia (0.025 mg/kg body weight, intraperitoneally) to be sacrificed, and then, the aortas were excised. The excised aortas were perfused with cold 0.1 M PBS (pH 7.4) and then fixed by a cold fixative, 4 % paraformaldehyde in 0.1 M PBS (pH 7.4). Each excised aorta was cut and placed onto glass slides. The dissected aortic root of the mice was embedded in Tissue-Tek medium (Sakura Finetechnical Co., Ltd., Tokyo, Japan) and frozen in isopentane/dry ice. Serial cross sections of 10-µm thickness for autoradiography study and 5-µm thickness for immunohistochemistry were cut immediately and thaw-mounted on glass slides. The other organs were also excised, and their radioactivities were measured using a Wizard 1480 gamma counter (PerkinElmer Life Sciences, Boston, MA).

Autoradiography Study

The excised and cryosections of aortas on glass slides were exposed to a phosphor imaging plate (Fuji Imaging Plate BAS-SR 2025, Fuji Photo Film Co., Ltd., Tokyo, Japan) together with a set of calibrated standards for about 12 h. After each exposure, the imaging plate was scanned with a computerized imaging analysis system (FLA 7000 Bio-Imaging Analyzer; Fuji Photo Film Co., Ltd.) and images were analyzed using Multi Gauge V3.2 (Fuji Photo Film Co., Ltd.).

Immunohistochemistry

Movat's pentachrome staining of serial aortic root sections was performed with previously reported procedure [17, 23]. Immunohistochemical staining of the serial sections with a mouse macrophage-specific antibody (Mac-2, clone m3/38, Cedarlane, Ontario, Canada) was performed in accordance with a previously reported immunohistochemical procedure [17, 24]. Briefly, the sections were treated with 3 % hydrogen peroxide to block the endogenous peroxide activity. Then, the primary antibodies (Mac-2, 1:500) were added to the sections and incubated with for 30 min at room temperature. The sections were washed twice with Tris-buffered saline, and then, Histofine Simple Stain (MAX-PO, Nichirei Bioscience, Gumma, Japan) and 3,3′-diaminobenzidine tetrahydrochloride (DAB) (Dako Japan, Tokyo, Japan) were used to visualize the bound primary antibody in the section by the avidin/biotin conjugate immunoperoxidase procedure. After counterstaining with hematoxylin, the sections were observed under a microscope (Biozero BZ-8000; KEYENCE Japan Co., Osaka, Japan).

Polarization of Macrophages

RAW264.7 mouse macrophages were purchased from ATCC (Rockville, MD) and cultured in DMEM with 10 % fetal bovine serum and penicillin (100 U/ml)–streptomycin (100 µg/ml) at 37 °C in a humidified atmosphere containing 5 % CO_2. RAW264.7 macrophages were polarized to M1 or M2 in accordance with a previously reported method with some modification [25]. In brief, the cells were cultured at 37 °C for 48 h in DMEM with stimulants [for M1, lipopolysaccharide (LPS, 10 nM) and interferon gamma (IFN-γ, 10 nM); for M2, interleukin-4 (IL-4) (40 nM)]. The polarizations were confirmed by evaluating the expressions of markers [for M1, inducible nitric oxide synthase (iNOS); for M2, mannose receptor (MR)] by quantitative RT-PCR analysis. Total RNA was extracted using ISOGEN reagent (Toyobo Co., Ltd., Osaka, Japan) and then transcribed using a ReverTra Ace® qPCR RT kit (Toyobo Co., Ltd.) with PCR Thermal Cycler Dice (Takara Bio Inc., Otsu, Japan). The acquired cDNA was quantified by real-time PCR analysis using the SYBR Green dye (Toyobo Co., Ltd.) and a 7500 real-time PCR system (Life Technologies, Carlsbad, CA, USA). The expression level of each messenger RNA (mRNA) was normalized to that of β-actin mRNA. The primer sets used in this study were as follows: β-actin 5′-CCCTGTATGCCTCTGGTC-3′ (forward), 5′-GTCT TTACGGATGTCAACG-3′ (reverse); iNOS 5′-CACGGAC-GAGACGGATAG-3′ (forward), 5′-GGGAGGAGCTGATG

GAGT-3′ (reverse); MR 5′-CTCGTGGATCTCCGTGA-CAC-3′ (forward), 5′-GCAAATGGAGCCGTCTGTGC-3′ (reverse) [25].

Cellular Uptake Study

RAW264.7 macrophages (1×10^6 cells) were cultured and polarized to M1 or M2 or nonpolarized (M0) by the method described above for 48 h in a 6-well dish (Becton Dickinson, Mountain View, CA). The cells were washed twice with PBS(−). [^{99m}Tc]IgG [100 kBq/0.1 μg/2 ml PBS(−)] was added to the cells, and the cells were incubated at 37 °C in a humidified atmosphere containing 5 % CO_2. After 1 h of incubation, the cells were washed three times with PBS(−) and lysed with 0.2 N NaOH. The radioactivity of the lysates was measured using a Wizard 1480 gamma counter (PerkinElmer Life Sciences, Boston, MA), and the cell lysate protein concentration was measured by the bicinchoninic acid (BCA) method (Thermo Fisher Scientific, Waltham, MA).

Western Blot Analysis

Cell lysates were prepared from M1, M2, and M0 RAW264.7 macrophages by homogenization in RIPA buffer (Thermo Fisher Scientific) containing 1 % protease inhibitor (P8340, Sigma-Aldrich Co., MO). The protein content of the lysates was determined by the BCA method (Thermo Fisher Scientific) using 5 μg of protein/lane. The lysates were subjected to electrophoresis on 5–20 % sodium dodecyl sulfate (SDS)-polyacrylamide gels, and the separated proteins were transferred to polyvinylidene difluoride membranes. After blocking with Blocking One (Nacalai Tesque, Inc., Kyoto, Japan), the membranes were incubated with a goat anti-mouse FcγRI antibody (AF2074, R&D Systems, Minneapolis, MN) or a goat anti-mouse FcγRII/RIII antibody (AF1460, R&D Systems) followed by horseradish peroxidase-conjugated donkey anti-goat IgG antibody (sc-2033, Santa Cruz Biotechnology, Santa Cruz, CA). The bands were visualized using Pierce™ ECL Plus Western Blotting Substrate (Thermo Fisher Scientific) with a LAS-4000 luminocapture instrument (Fuji Photo Film Co., Ltd.). β-Actin was used as a protein loading control.

Cellular Uptake of [^{99m}Tc]IgG Under Blockade of Fcγ Receptors

For the blocking study, M1 RAW264.7 macrophages (1×10^6 cells) were treated with an anti-FcγR antibody (553141, BD Biosciences, San Jose, CA) (0.1 mg/1 ml of PBS) for 15 min and [^{99m}Tc]IgG (100 kBq/0.1 μg/2 ml of PBS) was then added. After 1 h of incubation, the cells were washed three times with PBS and lysed with 0.2 N NaOH. The radioactivity of the lysates was measured using a Wizard 1480 gamma counter (PerkinElmer Life Sciences), and the cell lysate protein concentration was measured by the BCA method (Thermo Fisher Scientific).

Statistical Analysis

Data are presented as mean ± SD for the *in vivo* study and mean ± SEM for the *in vitro* studies. Results of the *in vivo* study (the radioactivity of apoE$^{-/-}$ mouse aorta vs that of C57BL/6J mouse aorta) and *in vitro* study (the radioactivity of FcγR-blocked M1 macrophages vs that of nonblocked M1 macrophages) were compared using unpaired Student's *t* test. Results of the *in vitro* studies (the cellular uptake study of [^{99m}Tc]IgG and the expression levels of FcγRs in M1, M2, and M0 macrophages) were statistically evaluated by one-way factorial ANOVA followed by the Tukey–Kramer test.

Results

Probe Preparation

[^{99m}Tc]IgG was acquired with a radiochemical yield of 31.8 ± 6.8 % (n = 3) and a radiochemical purity of over 99 % (n = 3) (Supplemental Fig. 1). The stability of [^{99m}Tc]IgG in mouse plasma was over 90 % for 24-h incubation.

In Vivo Study of [^{99m}Tc]IgG

The distributions of [^{99m}Tc]IgG in apoE$^{-/-}$ mice and C57BL/6J (wild type) mice in each organ 24 h after administration are shown at Table 1. The accumulation levels of [^{99m}Tc]IgG in the aortas were significantly higher in apoE$^{-/-}$ mice than in C57BL/6J mice (5.1 ± 1.3 vs 2.8 ± 0.5 %ID/g, $p < 0.05$), whereas the radioactivities of

Table 1. Biodistribution of [^{99m}Tc]IgG in apoE$^{-/-}$ or C57BL/6J (wild type) mice 24 h after administration

	ApoE$^{-/-}$	C57BL/6J
Aorta	5.1 ± 1.3	2.8 ± 0.5
Heart	1.6 ± 0.1	1.9 ± 0.3
Lung	2.2 ± 1.3	1.7 ± 1.4
Liver	4.6 ± 1.2	4.8 ± 0.8
Kidney	2.3 ± 0.5	2.3 ± 0.4
Stomach	1.5 ± 0.4	1.9 ± 0.6
Small intestine	1.4 ± 0.2	1.7 ± 0.2
Large intestine	3.5 ± 0.6	3.0 ± 0.3
Pancreas	0.7 ± 0.2	1.0 ± 0.1
Spleen	5.3 ± 0.8	6.9 ± 0.8
Brain	0.1 ± 0.0	0.1 ± 0.0
Muscle	0.6 ± 0.2	0.8 ± 0.1
White fat	0.3 ± 0.1	0.4 ± 0.1
Brown fat	1.3 ± 0.4	1.2 ± 0.3
Thyroid	1.9 ± 0.2	2.3 ± 0.3
Blood	15.8 ± 0.9	18.2 ± 2.0

The results are expressed as %ID/g (mean ± SD)

other organs were not significantly different between apoE$^{-/-}$ mice and wild-type mice.

Autoradiography and Histopathological Analysis

The distributions of [^{99m}Tc]IgG in apoE$^{-/-}$ and C57BL/6J mice aortas were evaluated by autoradiography (Fig. 1a, c). Autoradiography (ARG) images showed a heterogeneous distribution of [^{99m}Tc]IgG, and high radioactivity was found near the atherosclerotic lesions (Fig. 1a, b). On the other hand, the radioactivity derived from [^{99m}Tc]IgG was scarcely observed in the C57BL/6J mouse aortas (Fig. 1c, d). These findings indicate that [^{99m}Tc]IgG accumulated specifically in the atherosclerotic plaques in the apoE$^{-/-}$ mouse aortas. As for the study of aortic roots of apoE$^{-/-}$ or C57BL/6J mice, Movat's pentachrome staining revealed significant intimal thickening (Fig. 1e–j), which suggests that atherosclerotic plaques were formed in the intima of aortic roots. Macrophage-infiltrated areas of the plaques were detected by Mac-2 immunohistochemical staining (Fig. 1f), and the Mac-2-positive areas coincided with high-radioactivity areas observed by ARG (Fig. 1e). These findings suggest that [^{99m}Tc]IgG accumulates in the macrophage-infiltrated atherosclerotic plaques.

Cellular Uptake Study of [^{99m}Tc]IgG

The polarization of RAW264.7 macrophages to M1 or M2 was confirmed by quantitative RT-PCR analysis (Fig. 2). The iNOS expression level was significantly higher in the RAW264.7 macrophages stimulated with LPS and IFNγ, which suggests that they were M1 macrophages (Fig. 2a). On the other hand, the macrophages treated with IL-4 showed significantly higher MR expression levels, which suggests that they were M2 macrophages (Fig. 2b). As for the cellular uptake of [^{99m}Tc]IgG in each polarized macrophage type, M1 macrophages showed significantly higher levels of [^{99m}Tc]IgG than M2 or M0 macrophages [2.2 ± 0.3 (M1) vs 0.5 ± 0.1 (M2), 0.4 ± 0.1 (M0) %dose/mg protein, $p < 0.01$] (Fig. 3).

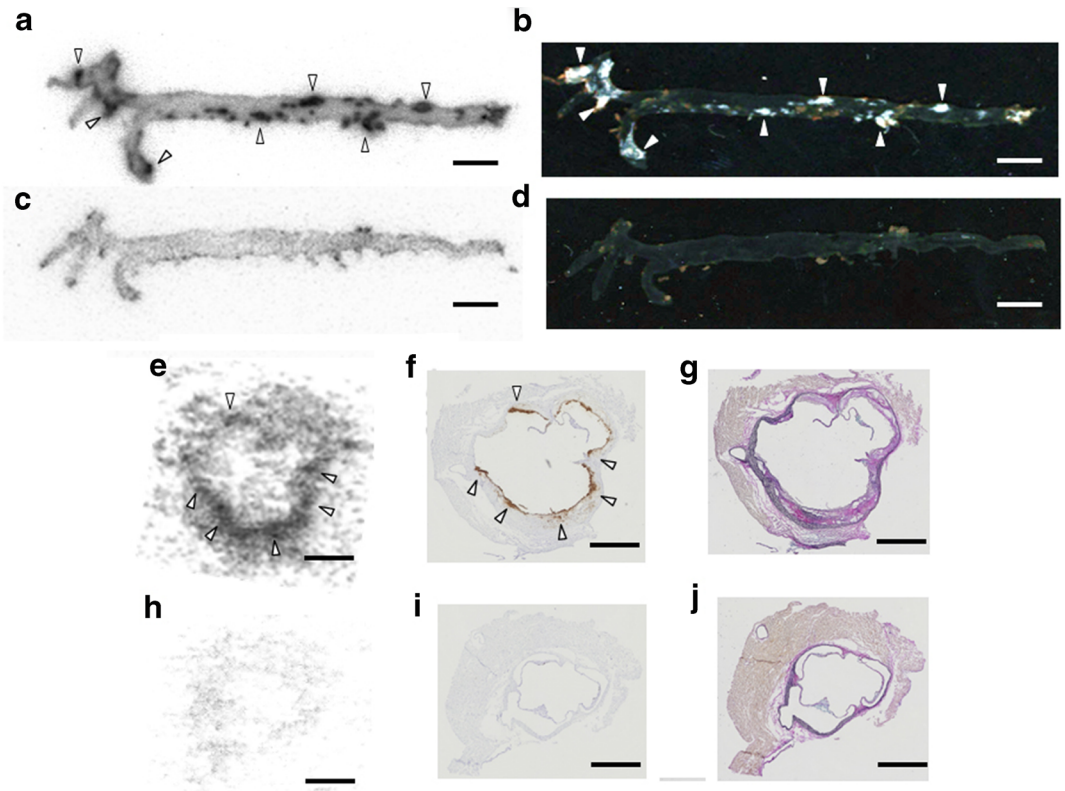

Fig. 1. Autoradiography (ARG) images of apoE$^{-/-}$ mice 24 h after [^{99m}Tc]IgG administration. **a** ARG and **b** bright-field images of aortas from apoE$^{-/-}$ mice and **c** ARG and **d** bright-field images of aortas from C57BL/6J (wild type) mice 24 h after injection of [^{99m}Tc]IgG. *Scale bar* represents 10 mm. **e** ARG and **f** Mac-2 (macrophage) immunohistochemical staining and **g** Movat's pentachrome staining images of aortic root of apoE$^{-/-}$ mice or **h** ARG and **i** Mac-2 (macrophage) immunohistochemical staining and **j** Movat's pentachrome staining of aortic root of C57BL/6J (**h**–**j**) mice 24 h after injection of [^{99m}Tc]IgG. *Scale bar* represents 0.5 mm.

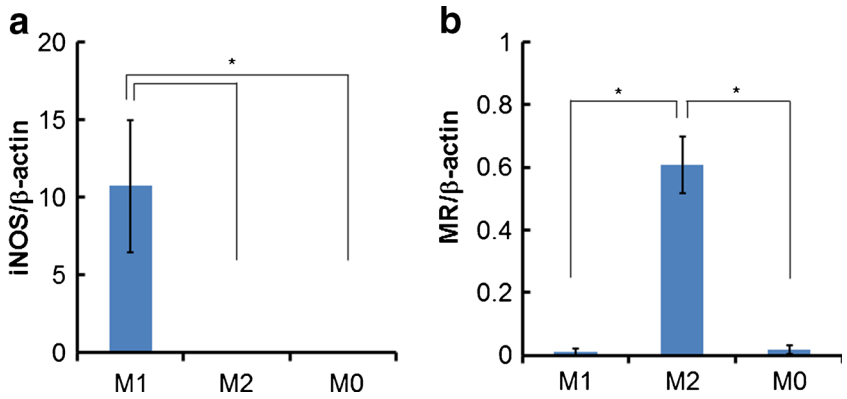

Fig. 2. **a** iNOS and **b** MR expression levels in RAW264.7 cells normalized by β-actin expression levels after treatment with LPS and IFN-γ (M1) or IL-4 (M2) or nontreatment (M0) determined by quantitative RT-PCR analysis. Data are expressed as iNOS per β-actin or MR per β-actin values (mean ± SEM). Comparison in each group was performed by one-way factorial ANOVA followed by the Tukey–Kramer test [*$p < 0.01$ vs M2 and M0 (**a**) or M1 and M0 (**b**)].

Fcγ Receptor Expression on Polarized Macrophages

As shown in Fig. 4, the expression levels of FcγRs on each type of polarized macrophage were evaluated by western blot analysis. As a result, M1 macrophages showed higher expression levels of FcγRI and FcγRII than M2 and M0 macrophages [FcγRI/β-actin 2.5 ± 0.2 (M1) vs 1.6 ± 0.1 (M2), 1.4 ± 0.1 (M0); FcγRII/β-actin 1.9 ± 0.2 (M1) vs 1.3 ± 0.1 (M2), 0.9 ± 0.1 (M0)] (Fig. 4a–c). On the other hand, there was no significant difference among the macrophage subtypes in the expression level of FcγRIII [FcγRIII/β-actin 1.2 ± 0.1 (M1) vs 1.2 ± 0.1 (M2), 1.1 ± 0.1 (M0)] (Fig. 4a, d).

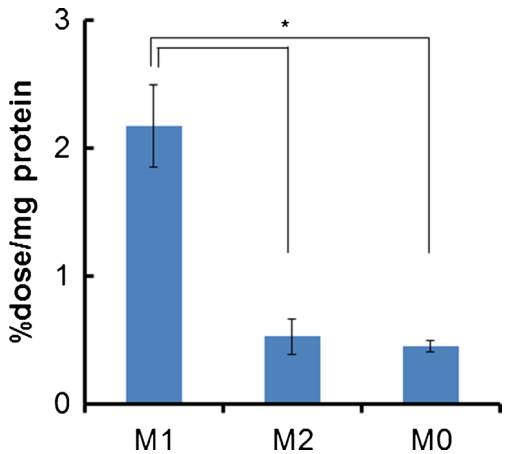

Fig. 3. Cellular uptake of [^{99m}Tc]IgG in M1, M2, or M0 macrophages 1 h after incubation. Data are expressed as %dose/mg protein (mean ± SEM). Comparison in each group was performed by one-way factorial ANOVA followed by the Tukey–Kramer test (*$p < 0.01$ vs M2 and M0).

Cellular Uptake of [^{99m}Tc]IgG Under Blockade of Fcγ Receptors

To evaluate whether [^{99m}Tc]IgG uptake in M1 macrophages depends on the FcγRs, the cellular uptake of [^{99m}Tc]IgG was studied with or without pretreatment with the anti-FcγR antibody. The [^{99m}Tc]IgG accumulation in M1 macrophages was significantly suppressed by pretreatment with the anti-FcγR antibody [2.2 ± 0.3 (nonpretreatment) vs 1.2 ± 0.2 (pretreatment) %ID/mg protein, $p < 0.01$] (Fig. 5).

Discussion

In this study, we first confirmed that radiolabeled non-targeting IgG ([^{99m}Tc]IgG) accumulated in atherosclerotic lesions, especially in macrophage-infiltrated areas in apoE$^{-/-}$ mice (Fig. 1). Furthermore, M1 macrophages showed a significantly higher uptake level of [^{99m}Tc]IgG than M2 macrophages or M0 macrophages (Fig. 3). These findings suggest that IgG itself was delivered to macrophages, especially in areas infiltrated by M1 macrophages in plaque lesions.

Macrophages have been reported to polarize to various types, especially M1 and M2 [26]. M1 macrophages, which are the classically activated macrophages, have pro-inflammatory properties; for example, they secrete pro-inflammatory cytokines and mediators. M2 macrophages, which are the alternatively activated macrophages, show anti-inflammatory properties, that is, they produce factors that suppress T cell proliferation and activities. In human and animal atherosclerosis models, M1 and M2 macrophages are reported to exist in atherosclerotic plaque lesions. For example, M1 macrophages are reported to be abundant in areas with high levels of lipids and to localize in areas that are distinct from those in which M2 macrophages localize in human atherosclerotic plaques [27]. Although the origin of

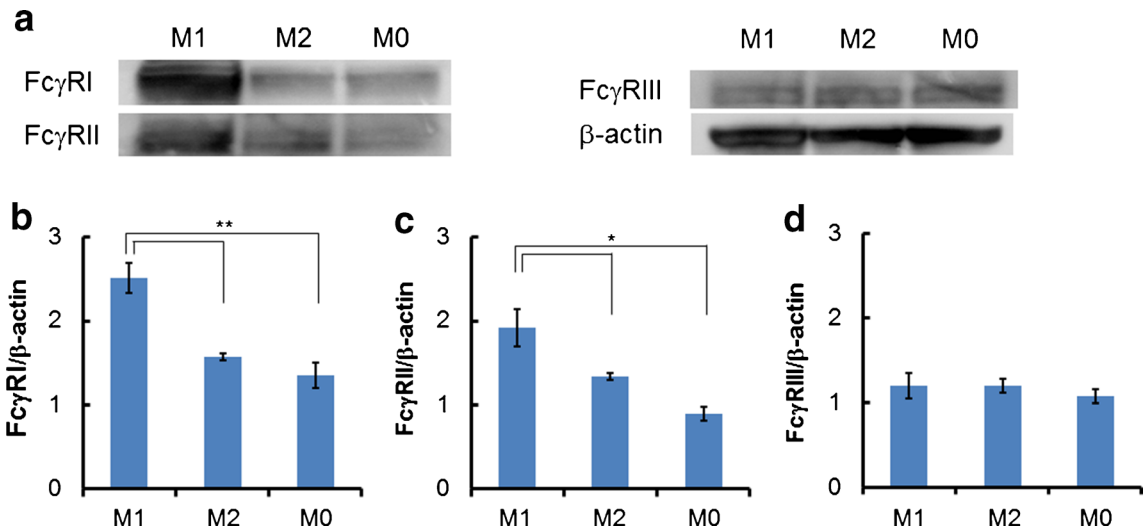

Fig. 4. Detection of expression of FcγRI, FcγRII, and FcγRIII on M1, M2, or M0 macrophages by western blot analysis. **a** Representative images of western blot analysis. Quantitative analysis of **b** FcγRI, **c** FcγRII, and **d** FcγRIII. Data are expressed as values for each FcγR per β-actin level (mean ± SEM). Comparison in each group was performed by one-way factorial ANOVA followed by the Tukey–Kramer test (*$p < 0.05$ and **$p < 0.01$ vs M2 and M0).

polarized macrophages and the mechanisms by which they are involved in the progression of atherosclerotic plaques are still unclarified, polarized macrophages may play critical roles in the development of atherosclerotic plaques [28]. Therefore, we examined the correlation between macrophage polarization and IgG accumulation and found that [^{99m}Tc]IgG was taken up especially in M1 macrophages (Fig. 3).

To clarify the mechanism of [^{99m}Tc]IgG accumulation in M1 macrophages, we next focused on the expression levels of FcγRs, which bind to the Fc domain of IgG and show high affinity (K_a = 10^7–10^9 M^{-1}) to IgG [29]. FcγRs allow macrophages to respond to products of adaptive immune systems, stimulate the production of cytokines in macrophages, and activate immune systems [30, 31]. Furthermore, intact IgG and Fc fragments were reported to localize at the inflammation sites of bacterial infection, whereas Fab fragments localize marginally [19]. Hence, FcγRs are supposed to be the main factor for [^{99m}Tc]IgG accumulation in M1 macrophages. Indeed, our study showed that the expression levels of FcγRI and FcγRII were higher in M1 macrophages than in M2 or M0 macrophages (Fig. 4). We also performed a cellular uptake study in which the FcγRs were inhibited by the anti-FcγR antibody. Although the blockade was not complete because the anti-FcγR antibody used in this study mainly binds to FcγRII and FcγRIII and has a relatively low affinity to FcγRI, the accumulation of [^{99m}Tc]IgG in M1 macrophages was significantly suppressed by the pretreatment with the anti-FcγR antibody (Fig. 5). These findings suggest that IgG itself is accumulated in M1 macrophages via FcγRs in the atherosclerotic plaques.

In the noninvasive imaging of atherosclerosis by PET/SPECT, 2-deoxy-2-[^{18}F]fluoro-D-glucose ([^{18}F]DG), a fluorine-18-labeled glucose analog, has been extensively studied and used for clinical diagnosis [6]. [^{18}F]DG enables the visualization of macrophage-infiltrated atherosclerotic plaques since [^{18}F]DG accumulates in cells with enhanced energy metabolism [32]. In addition, [^{18}F]DG has recently been reported to accumulate in M1 macrophages [33]. However, there are some limitations in the imaging of atherosclerotic plaques using [^{18}F]DG since [^{18}F]DG uptake is affected by blood glucose level and renal function [34, 35]. Hence, further studies have been performed to develop PET/SPECT imaging probes for visualizing atherosclerotic plaques with high sensitivity and specificity [8]. Over the past few decades, recombinant antibodies such as single-

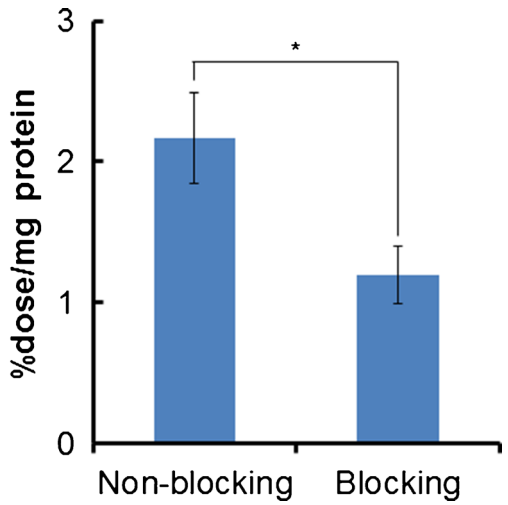

Fig. 5. Cellular uptake of [^{99m}Tc]IgG in M1 macrophages 1 h after incubation with or without pretreatment with anti-FcγR antibody. Data are expressed as %dose/mg protein (mean ± SEM). Comparison in each group was performed by the Student's *t* test (*$p < 0.01$ vs blocking group).

chain Fv (scFv), nanobodies, and diabodies have been generated [36]. These antibodies are designed to minimize the IgG structure without the loss of binding affinity to antigens, which leads to the rapid clearance from blood compared with IgG. In addition, they do not have the Fc domain, which is favorable for the escape from the target-independent accumulation in macrophages infiltrating in atherosclerotic plaques, as shown in this study. Indeed, nanobody-based imaging probes (ex. [^{99m}Tc]anti-vascular cell adhesion molecule-1 (VCAM1) nanobodies) have been developed and have shown good properties for the diagnosis of atherosclerosis [37]. Thus, those recombinant antibodies are promising base compounds for use in atherosclerosis imaging probes.

IgG was reported to accumulate in atherosclerotic plaques in animal models; however, the cell type visualized in the atherosclerotic lesions using radiolabeled IgG remains unclear [15]. In this study, we found that radiolabeled IgG accumulated specifically in M1 macrophages, which indicates that radiolabeled IgG can be used for visualizing inflammatory atherosclerotic lesions where [^{18}F]DG mainly accumulates. Thus, radiolabeled IgG may be used similarly to [^{18}F]DG for *in vivo* imaging of inflammatory lesions. [^{18}F]DG has been used clinically for the diagnosis of atherosclerosis; however, it is difficult to detect coronary atherosclerosis since the background myocardial uptake of [^{18}F]DG is greater than any signal derived from coronary plaques [5]. On the other hand, [^{99m}Tc]IgG showed lower accumulation levels in the apoE$^{-/-}$ mouse heart than in the apoE$^{-/-}$ mouse aorta in this study (heart 1.6 ± 0.1; aorta 5.1 ± 1.3 %ID/g), which is preferable for visualizing coronary atherosclerosis. In addition, the IgG distribution would not be affected by systemic conditions such as blood glucose levels as in the case of [^{18}F]DG. Therefore, radiolabeled IgG would be a more favorable probe for the diagnosis of coronary atherosclerosis in addition to that of the carotid artery. Furthermore, several studies demonstrated that [^{18}F]DG can be used for the precise evaluation of the therapeutic efficacy of antihyperlipidemic agents such as statin in the treatment of atherosclerosis [38, 39]. Therefore, [^{99m}Tc]IgG may also be a potential probe for evaluating the therapeutic efficacy of agents for atherosclerosis. However, [^{99m}Tc]IgG showed a long half-life in serum (artery-to-blood ratio 24 h after injection in apoE$^{-/-}$ mice 0.32 ± 0.09). This feature would be unfavorable for the SPECT imaging of atherosclerosis because a higher rate of clearance from blood is necessary for the rapid high-contrast imaging of the target pathological lesion [40]. The accumulation of IgG in inflammatory atherosclerotic lesions would be via FcγRs expressed on M1 macrophages, as confirmed by this study. This suggests that the key factor for IgG accumulation is the Fc domain of IgG. Previously, it was reported that a radiolabeled Fc fragment, prepared by IgG digestion and had a molecular weight one third that of IgG, could be used for the diagnosis of inflammation [16]. Thus, our study also suggests the possibility of using a radiolabeled Fc fragment for visualizing active inflammatory atherosclerotic plaques. In this study, we were unable to clarify the extent to which the PET/SPECT imaging of atherosclerosis using IgG-based probes is affected by the expression of FcγRs on the inflammatory macrophages infiltrating into atherosclerotic plaques, compared with the expression of the biomolecule targeted by the IgG-based probes. Therefore, to determine whether a radiolabeled Fc fragment is a useful probe for the diagnosis of atherosclerosis, especially active inflammatory atherosclerotic lesions, it would be necessary to estimate how a radiolabeled Fc fragment accumulates in atherosclerotic lesions depending on the FcγR expression levels. The expression levels of FcγRs should also be compared with those of other biomolecules that are the targets of the previously reported IgG-based probes. Thus, the preparation of radiolabeled Fc fragments and studies on these issues are now in progress.

Conclusions

In this study, we found that radiolabeled IgG accumulated in pro-inflammatory M1 macrophages, probably via FcγRs in atherosclerotic lesions. This finding suggests that imaging probes based on IgG enable the visualization of active inflammatory atherosclerotic lesions independent of the target biomolecules of IgG. This feature should be taken into account in the diagnosis of atherosclerosis using IgG-based probes.

Acknowledgements. This study was supported by JSPS KAKENHI (Grant Numbers 26293268, 15K15440, 24890003, and 26860961) and the Creation of Innovation Centers for Advanced Interdisciplinary Research Areas Program, Ministry of Education, Culture, Sports, Science and Technology, Japan.

Compliance with Ethical Standards

Conflict of Interest

N.T. has grant support from Hitachi, Ltd. H.H. and T.S. are employees of Hitachi Ltd. The other authors declare that there is no conflict of interest associated with this manuscript.

References

1. Falk E, Shah PK, Fuster V (1995) Coronary plaque disruption. Circulation 92:657–671
2. Hanzawa H, Sakamoto T, Kaneko A et al (2015) Combined plasma and tissue proteomic study of atherogenic model mouse: approach to elucidate molecular determinants in atherosclerosis development. J Proteome Res 14:4257–4269
3. Wang X, Connolly TM (2010) Biomarkers of vulnerable atheromatous plaques: translational medicine perspectives. Adv Clin Chem 50:1–22
4. Sakamoto T, Hanzawa H, Manri N et al (2016) Discovery and evaluation of biomarkers for atherosclerosis. In: Kuge Y, Shiga T, Tamaki N (eds) Perspectives on nuclear medicine for molecular diagnosis and integrated therapy. Springer Japan, Sapporo, pp. 131–139
5. Tarkin JM, Joshi FR, Rudd JH (2014) PET imaging of inflammation in atherosclerosis. Nat Rev Cardiol 11:443–457
6. Bucerius J, Hyafil F, Verberne HJ et al (2016) Position paper of the Cardiovascular Committee of the European Association of Nuclear

Medicine (EANM) on PET imaging of atherosclerosis. Eur J Nucl Med Mol Imaging 43:780–792
7. Libby P, Ridker PM, Maseri A (2002) Inflammation and atherosclerosis. Circulation 105:1135–1143
8. Shimizu Y, Kuge Y (2016) Recent advances in the development of PET/SPECT probes for atherosclerosis imaging. Nucl Med Mol Imaging 50:284–291
9. Temma T, Saji H (2012) Radiolabelled probes for imaging of atherosclerotic plaques. Am J Nucl Med Mol Imaging 2:432–447
10. Nakamura I, Hasegawa K, Wada Y, Hirase T, Node K, Watanabe Y (2013) Detection of early stage atherosclerotic plaques using PET and CT fusion imaging targeting P-selectin in low density lipoprotein receptor-deficient mice. Biochem Biophys Res Commun 433:47–51
11. Temma T, Ogawa Y, Kuge Y et al (2010) Tissue factor detection for selectively discriminating unstable plaques in an atherosclerotic rabbit model. J Nucl Med 51:1979–1986
12. Kuge Y, Takai N, Ogawa Y et al (2010) Imaging with radiolabelled anti-membrane type 1 matrix metalloproteinase (MT1-MMP) antibody: potentials for characterizing atherosclerotic plaques. Eur J Nucl Med Mol Imaging 37:2093–2104
13. Larson SM (1985) Radiolabeled monoclonal anti-tumor antibodies in diagnosis and therapy. J Nucl Med 26:538–545
14. McCafferty J, Griffiths AD, Winter G, Chiswell DJ (1990) Phage antibodies: filamentous phage displaying antibody variable domains. 348:552–554
15. Demacker PN, Dormans TP, Koenders EB, Corstens FH (1993) Evaluation of indium-111-polyclonal immunoglobulin G to quantitate atherosclerosis. J Nucl Med 34:1316–1321
16. Fischman AJ, Rubin RH, Khaw BA et al (1989) Radionuclide imaging of experimental atherosclerosis with nonspecific polyclonal immunoglobulin G. J Nucl Med 30:1095–1100
17. Shimizu Y, Hanzawa H, Zhao Y et al (2016) Radioimmunodetection of atherosclerotic lesions focusing on the accumulation mechanism of immunoglobulin G. In: Kuge Y, Shiga T, Tamaki N (eds) Perspectives on nuclear medicine for molecular diagnosis and integrated therapy. Springer Japan, Sapporo, pp. 141–150
18. De Gersem R, Jamar F (2010) Nonspecific human immunoglobulin G for imaging infection and inflammation: what did we learn? The quarterly journal of nuclear medicine and molecular imaging : official publication of the Italian Association of Nuclear Medicine (AIMN) [and] the International Association of Radiopharmacology (IAR), [and] Section of the So 54:617–628
19. Fischman AJ, Rubin RH, White JA et al (1990) Localization of Fc and Fab fragments of nonspecific polyclonal IgG at focal sites of inflammation. J Nucl Med 31:1199–1205
20. Abrams MJ, Juweid M, tenKate CI et al (1990) Technetium-99m-human polyclonal IgG radiolabeled via the hydrazino nicotinamide derivative for imaging focal sites of infection in rats. J Nucl Med 31:2022–2028
21. Ono M, Arano Y, Mukai T et al (2001) Plasma protein binding of (99 m)Tc-labeled hydrazino nicotinamide derivatized polypeptides and peptides. Nucl Med Biol 28:155–164
22. Larsen SK, Solomon HF, Caldwell G, Abrams MJ (1995) [99mTc]tricine: a useful precursor complex for the radiolabeling of hydrazinonicotinate protein conjugates. Bioconjug Chem 6:635–638
23. Vucic E, Dickson SD, Calcagno C et al (2011) Pioglitazone modulates vascular inflammation in atherosclerotic rabbits noninvasive assessment with FDG-PET-CT and dynamic contrast-enhanced MR imaging. JACC Cardiovasc Imaging 4:1100–1109
24. Zhao Y, Kuge Y, Zhao S et al (2007) Comparison of 99mTc-annexin A5 with 18F-FDG for the detection of atherosclerosis in ApoE−/− mice. Eur J Nucl Med Mol Imaging 34:1747–1755
25. Zhang B, Wang J, Gao J et al (2009) Alternatively activated RAW264.7 macrophages enhance tumor lymphangiogenesis in mouse lung adenocarcinoma. J Cell Biochem 107:134–143
26. Mantovani A, Sica A, Sozzani S, Allavena P, Vecchi A, Locati M (2004) The chemokine system in diverse forms of macrophage activation and polarization. Trends Immunol 25:677–686
27. Chinetti-Gbaguidi G, Baron M, Bouhlel MA et al (2011) Human atherosclerotic plaque alternative macrophages display low cholesterol handling but high phagocytosis because of distinct activities of the PPARgamma and LXRalpha pathways. Circ Res 108:985–995
28. Moore KJ, Sheedy FJ, Fisher EA (2013) Macrophages in atherosclerosis: a dynamic balance. Nat Rev Immunol 13:709–721
29. van de Winkel JG, Anderson CL (1991) Biology of human immunoglobulin G Fc receptors. J Leukoc Biol 49:511–524
30. Anderson CF, Mosser DM (2002) Cutting edge: biasing immune responses by directing antigen to macrophage Fc gamma receptors. J Immunol (Baltimore, Md : 1950) 168:3697–3701
31. Ravetch JV, Bolland S (2001) IgG Fc receptors. Annu Rev Immunol 19:275–290
32. Ogawa M, Ishino S, Mukai T et al (2004) ^{18}F-FDG accumulation in atherosclerotic plaques: immunohistochemical and PET imaging study. J Nucl Med 45:1245–1250
33. Satomi T, Ogawa M, Mori I et al (2013) Comparison of contrast agents for atherosclerosis imaging using cultured macrophages: FDG versus ultrasmall superparamagnetic iron oxide. J Nucl Med 54:999–1004
34. Ziegler WAWSI, Tho'dtmann R, Hanauske A-R, Schwaiger M (1999) Reproducibility of metabolic measurements in malignant tumors using FDG PET. J Nucl Med 40:1771–1777
35. Zhao Y, Zhao S, Kuge Y, Tamaki N (2013) Elevated ^{18}F-FDG levels in blood and organs after angiotensin II receptor blocker administration: experiment in mice administered telmisartan. J Nucl Med 54:1384–1388
36. Cuesta AM, Sainz-Pastor N, Bonet J, Oliva B, Alvarez-Vallina L (2010) Multivalent antibodies: when design surpasses evolution. Trends Biotechnol 28:355–362
37. Broisat A, Hernot S, Toczek J et al (2012) Nanobodies targeting mouse/human VCAM1 for the nuclear imaging of atherosclerotic lesions. Circ Res 110:927–937
38. Ogawa M, Magata Y, Kato T et al (2006) Application of ^{18}F-FDG PET for monitoring the therapeutic effect of antiinflammatory drugs on stabilization of vulnerable atherosclerotic plaques. J Nucl Med 47:1845–1850
39. Zhao Y, Fukao K, Zhao S et al (2015) Irbesartan attenuates atherosclerosis in Watanabe heritable hyperlipidemic rabbits: noninvasive imaging of inflammation by 18F-fluorodeoxyglucose positron emission tomography. Mol Imaging 14. doi:10.2310/7290.2015.00004
40. Romer T, Leonhardt H, Rothbauer U (2011) Engineering antibodies and proteins for molecular in vivo imaging. Curr Opin Biotech 22:882–887